Theory of core-level spectra in x-ray photoemission of pristine and doped graphene

V. Despoja[1,2,3,*] and M Šunjić[1,2]

[1]*Department of Physics, University of Zagreb, Bijenička 32, HR-10000 Zagreb, Croatia*

[2]*Donostia International Physics Center (DIPC), Paseo de Manuel de Lardizabal 4, 20018, San Sebastian, Spain*

[3]*Centro de Fisica de Materiales CSIC-UPV/EHU-MPC, Paseo de Manuel de Lardizabal 5, 20018, San Sebastian, Spain*

(Received 27 October 2013; published 11 December 2013)

Spectra of the C1s core hole, created in x-ray photoemission and screened by electronic excitations in pristine and doped graphene are calculated and discussed. We find that singular effects in the lineshapes are not possible in the pristine graphene, and their observation should be connected with the doping. However, the structure of the low-energy excitation spectrum in the region where the singular behavior is expected leads to asymmetries in the core-hole lineshapes in pristine graphene similar to those in doped graphene. This makes the analysis more complex than in the case of metals and may lead to an incorrect or incomplete interpretation of the experimental results.

DOI: 10.1103/PhysRevB.88.245416 PACS number(s): 73.20.Mf

I. INTRODUCTION

The excitation of localized levels in solids, especially in metals, can lead to a variety of many-body scattering processes, as can be revealed, e.g., in x-ray photoemission spectra from these levels. These phenomena and the information that they provided about the structure and local dynamics of electrons in such systems were among the reasons that they were extensively studied since the pioneering theoretical[1–10] and experimental[11,12] studies. The observation of asymmetric lineshapes was often used as an indicator of the metallicity of the system. The extension of these studies to new materials, like graphene, led to renewed interest in the application and interpretation of various spectroscopies to these systems. In this paper we therefore provide a theoretical prediction of the core-level photoemission spectra from pristine and doped graphene, discuss in detail the core-level lineshapes, and the possibility that they reveal singular behavior, as is the case in metals.

In Sec. II we briefly derive expressions for a localized level spectrum, corresponding to the $1s$ level of carbon, interacting with electronic excitations, which are described by the nonlocal dynamically screened Coulomb interaction. We shall neglect extrinsic (photoelectron) scattering processes, in which case the measured photoelectron spectrum corresponds to the core-hole spectrum. In Sec. III we present an analytic discussion of possible singularities in x-ray photoemission (XPS) lineshapes using asymptotic expressions for the singularity index, and conclude that they can occur only in doped graphene. This may in principle open the possibility to directly connect doping and line asymmetry, but later in a more exact calculation we show the restricted validity of these asymptotic results. In Sec. IV we present methodology we use in the calculation of the propagator of dynamically screened Coulomb interaction in graphene. With this full propagator in Sec. V we calculate singularity indices in pristine and doped graphene and compare them to the previous approximate results. We show that, unlike the situation in the metals, the singularity indices α vary in a much more complicated way. For $\omega = 0$ they indeed start from their asymptotic values, but soon the reverse situation occurs: In pristine graphene α increases above the value in doped graphene, which decreases until it reaches the two-dimensional (2D) plasmon peak. The fact is that E_F, the hole decay linewidth, the pair, and plasmon energies all lie in the same energy region, so that detailed calculations become necessary. In Sec. VI we present a method for the calculation of the complete core-hole spectrum and its various properties. In Sec. VII we use this method to calculate and discuss the shapes and properties of C1s core-hole spectra in graphene. We also compare them to the existing experimental results, pointing out a possible incorrect interpretation of measured C1s core-hole lineshapes in XPS.

II. DERIVATION OF THE LOCALIZED LEVEL SPECTRUM

In Fig. 1 we show schematically the geometry of the system. The center of the quasi-two-dimensional graphene layer is at the $z = 0$ plane, and the core hole is created at some point $\mathbf{R} = (\boldsymbol{\rho}, z)$, to be defined later, with the wave function $u(\mathbf{r} - \mathbf{R})$. In this way our formalism can also be applied to study spectra of atoms adsorbed at various positions on graphene.

The Hamiltonian of the system is

$$H = H_0 + H_{\text{int}},$$

where

$$H_0 = E_0 d^+ d + \sum_{\mathbf{K}n} E_{\mathbf{K}n} c^+_{\mathbf{K}n} c_{\mathbf{K}n}, \tag{1}$$

E_0 and d^+ are the energy and the creation operator of a C1s core state, and $C^+_{\mathbf{K}n}$ creates the electrons in graphene with energy $E_{\mathbf{K}n}$ and the wave function $\Phi_{n\mathbf{K}}(\boldsymbol{\rho}, z)$. $\mathbf{K}$ represents the parallel wave vector and n is the conduction/valence band quantum number. The interaction Hamiltonian contains two terms

$$H_{\text{int}} = V_1 + V_2,$$

where

$$V_1 = d d^+ \sum_{ij} w_{i,j} c^+_i c_j \tag{2}$$

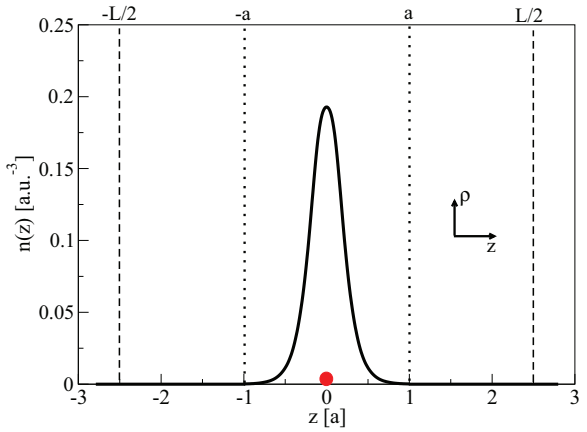

FIG. 1. (Color online) Local density approximation (LDA) graphene electronic pseudodensity averaged over xy plane. L is the thickness of one supercell. Scale on the abscissa is the unit cell parameter in xy plane $a = 4.651$ a.u. Red dot represents the core-hole position.

represents the interaction of the core hole with conduction/valence electrons in graphene, and

$$V_2 = \sum_{ijkl} v_{ijkl} c_i^+ c_j^+ c_k c_l \tag{3}$$

represents the electron-electron interaction in graphene. In the last two formulas we introduced shorter notation for the quantum numbers $i = (\mathbf{K},n)$. The matrix elements are

$$w_{ij} = \int d\mathbf{r} \psi_i^*(\mathbf{r}) U(\mathbf{r},\mathbf{R}) \psi_j(\mathbf{r}),$$
$$v_{ijkl} = \int d\mathbf{r} d\mathbf{r}' \psi_i^*(\mathbf{r}) \psi_j^*(\mathbf{r}') v(\mathbf{r},\mathbf{r}') \psi_k(\mathbf{r}') \psi_l(\mathbf{r}),$$

with

$$U(\mathbf{r},\mathbf{R}) = \int d\mathbf{r}' v(\mathbf{r},\mathbf{r}') |u(\mathbf{r}' - \mathbf{R})|^2.$$

The core-hole Green's function can be written as

$$G(t) = -i\theta(t)\, e^{-iE_0 t}\ \langle d\,|U(t,0)|\,d\rangle\,,$$

where $|d\rangle$ is a one-hole state with the binding energy E_0 in the interacting Fermi sea of graphene electrons, and $U(t,0)$ is the evolution operator in the interaction representation, or as

$$G(t) = -i\theta(t)\, e^{-iE_0 t}\ e^{\Phi(t)},$$

where $\Phi(t)$ is the sum of the cumulants[13,14]

$$\Phi(t) = \phi(t) + \phi_d(t).$$

$\phi_d(t)$ describes all processes responsible for the eventual core-hole decay (Auger, radiative decay, etc.), and is usually given in the form

$$\phi_d(t) = e^{-\gamma|t|},$$

where γ is the decay constant. $\phi(t)$ represents the core-hole interaction with the graphene electrons, which leads to characteristic structures in the hole spectrum: the energy shift, satellite structures, and so on.

In the following we shall make use of the formalism developed bythe authors of Ref. 13 to study XPS spectrum from

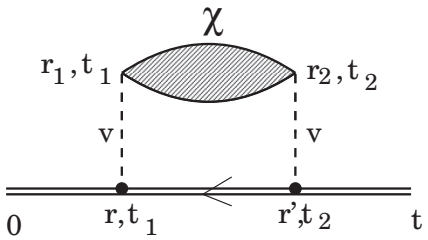

FIG. 2. The lowest-order cumulant in the XPS process.

localized levels in the vicinity of metallic surfaces, following earlier work on bulk metals.[1–10] For the localized hole only the lowest-order cumulant, shown in Fig. 2, is finite. Here $v(\mathbf{r}-\mathbf{r}')$ is the bare Coulomb interaction and χ is the exact response function of graphene electrons that can be written as

$$\chi(\mathbf{r}_1,\mathbf{r}_2,t_1,t_2) = \int_{-\infty}^{\infty} \frac{d\omega}{2\pi} e^{-i\omega t}\ \chi(\mathbf{r}_1,\mathbf{r}_2,\omega).$$

In the expansion shown in Fig. 2 we neglect the processes where the core hole directly couples to the excited electron-hole pair, as, e.g., in Fig. 3. The exact response function χ can be obtained as an infnite sum of the diagrams shown in Fig. 4. Here χ_0 describes the excitation and annihilation of an electron-hole pair created by the V_1 potential, and in principle includes all their scattering processes due to the V_2 potential. In the spirit of Random Phase Approximation (RPA) we shall take only the lowest-order term, shown in Fig. 5. From the diagram in Fig. 2 we obtain

$$\phi(t) = i \int_0^t dt_1 \int_0^{t_1} dt_2 \int d\mathbf{r} \int d\mathbf{r}' \int d\mathbf{r}_1 \int d\mathbf{r}_2,$$
$$|u(\mathbf{r}-\mathbf{R})|^2 v(\mathbf{r}-\mathbf{r}_1)\chi(\mathbf{r}_1,\mathbf{r}_2,t_1,t_2)v(\mathbf{r}_2-\mathbf{r}')|u(\mathbf{r}'-\mathbf{R})|^2. \tag{4}$$

If we notice that the induced part of the nonlocal interaction in the Fermi sea can be written as

$$W^{\rm ind}(\mathbf{r},\mathbf{r}',\omega) = \int d\mathbf{r}_1 \int d\mathbf{r}_2\ v(\mathbf{r}-\mathbf{r}_1)\chi(\mathbf{r}_1,\mathbf{r}_2,\omega)v(\mathbf{r}_2-\mathbf{r}'), \tag{5}$$

we find after integration over interaction times

$$\phi(t) = i \int_{-\infty}^{\infty} \frac{d\omega}{2\pi}\ f(\omega,t) \int d\mathbf{r} \int d\mathbf{r}'$$
$$\times |u(\mathbf{r}-\mathbf{R})|^2 W^{\rm ind}(\mathbf{r},\mathbf{r}',\omega)|u(\mathbf{r}'-\mathbf{R})|^2, \tag{6}$$

where

$$f(\omega,t) = \frac{it}{\omega} + \frac{1}{\omega^2}(e^{-i\omega t} - 1) \tag{7}$$

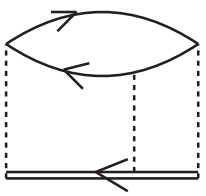

FIG. 3. Processes in which the hole interacts with the excited electron-hole pair.

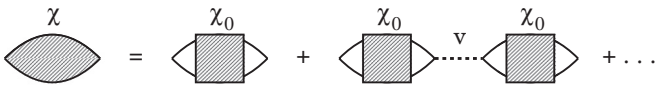

FIG. 4. Interacting electrons response function.

is a typical factor characteristic for the spectrum of a structureless hole. The first term will give the energy shift of the elastic (no-loss) line, the second leads to inelastic structures and provides the spectrum normalization. Because the hole dimension is very small compared to the screening length in graphene we can approximate

$$|u(\mathbf{r}-\mathbf{R})|^2 = \delta(\mathbf{r}-\mathbf{R})$$

and the cumulant becomes

$$\phi(\mathbf{R},t) = i\int_{-\infty}^{\infty}\frac{d\omega}{2\pi}\, f(\omega,t)\, W^{\rm ind}(\mathbf{R},\mathbf{R},\omega). \tag{8}$$

For the two-dimensional periodic lattice of graphene, defined by the inverse lattice vectors $\mathbf{G}$, we can write

$$W^{\rm ind}(\mathbf{R},\mathbf{R},\omega) = \int\frac{d\mathbf{Q}}{(2\pi)^2}\sum_{\mathbf{G}} e^{i\mathbf{G}\boldsymbol{\rho}}\, W^{\rm ind}_{\mathbf{G}}(\mathbf{Q},z,z,\omega). \tag{9}$$

The calculation of the response function χ and the induced potential $W^{\rm ind}$ in graphene is presented in Sec. IV B. If we define the spectral function

$$S_{\mathbf{G}}(\mathbf{Q},z,\omega) = -\frac{1}{\pi\, v_{\mathbf{Q}+\mathbf{G}}}\,{\rm Im}\left\{W^{\rm ind}_{\mathbf{G}}(\mathbf{Q},z,z,\omega)\right\}, \tag{10}$$

where $v_{\mathbf{Q}+\mathbf{G}} = \frac{2\pi}{|\mathbf{Q}+\mathbf{G}|}$ we can write

$$\phi(\mathbf{R},t) = \int_0^{\infty} d\omega\, f(\omega,t)\sum_{\mathbf{G}} e^{i\mathbf{G}\boldsymbol{\rho}}\int\frac{d\mathbf{Q}}{(2\pi)^2} v_{\mathbf{Q}+\mathbf{G}} S_{\mathbf{G}}(\mathbf{Q},z,\omega). \tag{11}$$

Using Eqs. (7) and (11) the core-hole Green's function can be written as

$$G(\mathbf{R},t) = -i\theta(t) e^{-i(\tilde{E}(\mathbf{R})-i\gamma)t} e^{\tilde{\phi}(\mathbf{R},t)}, \tag{12}$$

where

$$\tilde{\phi}(\mathbf{R},t) = \int_0^{\infty}\frac{d\omega}{\omega}\,\alpha(\mathbf{R},\omega)[e^{-i\omega t}-1] \tag{13}$$

generates inelastic structures in the spectrum and $\tilde{E}(\mathbf{R}) = E_0 + \Delta E(\mathbf{R})$ where

$$\Delta E(\mathbf{R}) = \int_0^{\infty} d\omega\,\alpha(\mathbf{R},\omega) \tag{14}$$

is the position-dependent core-hole energy shift. Here we also defined the new function, dynamical singularity index

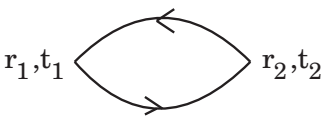

FIG. 5. Lowest-order process in the expansion of χ_0.

(sometimes also called asymmetry parameter)

$$\alpha(\mathbf{R},\omega) = \frac{1}{\omega}\sum_{\mathbf{G}_\parallel} e^{i\mathbf{G}_\parallel\boldsymbol{\rho}}\int\frac{d\mathbf{Q}}{(2\pi)^2}\, v_{\mathbf{Q}+\mathbf{G}_\parallel} S_{\mathbf{G}_\parallel}(\mathbf{Q},z,\omega). \tag{15}$$

Finally the core-hole spectrum is given by

$$A(\mathbf{R},\omega) = \frac{1}{2\pi}\int_{-\infty}^{\infty} dt\; e^{i(\omega-\tilde{E}(\mathbf{R}))t} e^{-\gamma|t|} e^{\tilde{\phi}(\mathbf{R},t)}, \tag{16}$$

which is also normalized

$$\int d\omega A(\mathbf{R},\omega) = 1$$

and satisfies the spectral sum rule[14]

$$\int d\omega\omega A(\mathbf{R},\omega) = E_0. \tag{17}$$

III. ANALYTIC DISCUSSION OF POSSIBLE SINGULARITIES IN XPS LINESHAPES

In this section we shall estimate the possibility to find singular lineshapes in the localized level (i.e., C1s) lineshapes in graphene (or any similar system where electrons form a Dirac cone). The relevant quantity is the density of electronic excitations $\rho(\omega)$ near the Fermi level. If we assume a fully screened (contact) potential V, the dynamical singularity index $\alpha(\omega)$ in Eq. (15) can be reduced to

$$\alpha_0(\omega) = \frac{1}{\omega}|V|^2\rho(\omega) \sim \omega^{\beta}, \tag{18}$$

which determines the shape of the inelastic contributions to the spectrum.[14,19] The density of states per unit area of electrons in the Dirac cone, with energies $E_{\mathbf{K}} = v|\mathbf{K}|$, for both spin directions is

$$g(E) = \frac{2}{\omega_0^2}E, \tag{19}$$

where $\omega_0 = \sqrt{2\pi}\hbar v/a_0$ and a_0 is the Bohr radius. For graphene $\omega_0 = 47.19$ eV. The density of excitations (without spin flip) is given by

$$\rho(\omega) = \frac{1}{2}\int_{E<E_F,\,E+\omega>E_F} g(E)g(E+\omega)dE.$$

In pristine (undoped graphene) $E_F = 0$, so using Eq. (19) the density of interband transitions becomes

$$\rho(\omega) = N\int_{-\omega}^{0} E(E+\omega)dE = \frac{N}{6}\,\omega^3, \tag{20}$$

where $N = \frac{2}{\omega_0^4}$. The predicted inelastic spectrum for this case ($\beta = 2$) goes to zero at the elastic line, which is not destroyed by electron scattering.[14] In the case of doped graphene, $E_F > 0$, we distinguish two regions. For $\omega < E_F$ only intraband transitions are possible, with the density

$$\rho(\omega) = N\int_{E_F-\omega}^{E_F} E(E+\omega)dE = N\left(E_F^2\omega - \frac{1}{6}\omega^3\right);\quad \omega < E_F. \tag{21}$$

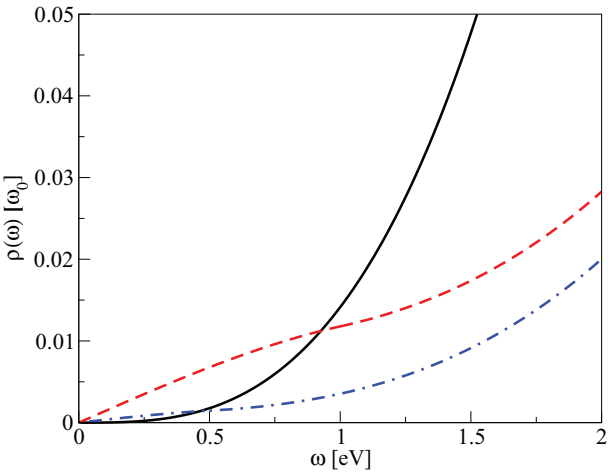

FIG. 6. (Color online) Density of electronic excitations $\rho(\omega)$ in pristine graphene (solid line), doped graphene ($E_F = 0.5$ eV) (blue dotted-dashed line), and doped graphene ($E_F = 1$ eV) (red dashed line).

The linear term in ω in Eq. (21), i.e., for $\beta = 0$, can lead to singular low-energy scattering and therefore singular lineshapes. Higher transition energies $\omega > E_F$ are not interesting in this context, but now we can have both intraband and interband processes

$$\rho^{\text{intra}}(\omega) = N\int_0^{E_F} E(E+\omega)dE = N\left(\frac{1}{3}E_F^3 + \frac{1}{2}E_F^2\omega\right),$$

$$\rho^{\text{inter}}(\omega) = -N\int_{E_F-\omega}^{0} E(E+\omega)dE = N\left(\frac{1}{3}E_F^3 - \frac{1}{2}E_F^2\omega + \frac{1}{6}\omega^3\right);\quad \omega > E_F$$

or, taken together

$$\rho^{\text{intra}}(\omega) + \rho^{\text{inter}}(\omega) = N\left(\frac{2}{3}E_F^3 + \frac{1}{6}\omega^3\right);\quad \omega > E_F. \qquad (22)$$

The excitation densities are shown in Fig. 6, scaled by the characteristic energy ω_0. The singularity indices α_0, given by Eq. (18), are shown in Fig. 7 for several E_F, but in this case we can only illustrate their qualitative behavior because $|V|^2$ is not known in this asymptotic approximation. We shall need a full calculation to obtain quantitative results for $\alpha(\omega)$, given in Fig. 8. However, even this analysis indicates that we can expect singular behavior only in the spectra of doped graphene where $\alpha_0(\omega) \sim$ const. for $\omega \to 0$. In Sec. V we shall verify this conclusion by detailed calculations of $\alpha(\omega)$, using graphene wave functions and properly screened interaction potential, and show that this asymptotic result is strongly modified.

IV. DYNAMICALLY SCREENED COULOMB INTERACTION IN GRAPHENE

A. Ground-state calculation

In this section we briefly describe the calculation of the Kohn-Sham (KS) wave functions and energy levels (band structure) in a graphene monolayer which are used to calculate the independent electron response function. A schematic representation of a graphene monolayer is shown in Fig. 1. For electronic structure calculations we used plane-wave self-consistent field density functional theory (DFT) code (PWSCF), within the QUANTUM ESPRESSO (QE) package,[15] and the Perdew-Zunger local density approximation (LDA) for the exchange correlation (xc) potential.[16] An electronic temperature of $k_BT \approx 0.1$ eV was assumed to achieve convergence in the calculation of the KS wave functions, and all energies were then extrapolated to 0 K. The ground-state electronic density was calculated using a $12 \times 12 \times 1$ Monkhorst-Pack special K-point mesh, i.e., by using 19 special points in the irreducible Brillouin zone. In the PWSCF code we used the norm-conserving LDA-based pseudopotentials for carbon atoms,[17] and we found the energy spectrum to be convergent with a 50-Ry plane-wave cutoff. The graphene band structure along the high symmetry $\Gamma - K - M - \Gamma$ direction shown in Fig. 3 of Ref. 18 was calculated along the path with

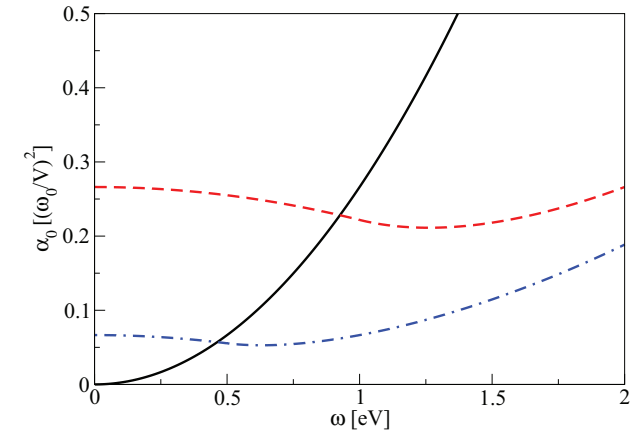

FIG. 7. (Color online) Singularity index $\alpha_0(\omega)$ in pristine graphene (solid line), doped graphene ($E_F = 0.5$ eV) (blue dotted-dashed line), and doped graphene ($E_F = 1$ eV) (red dashed line).

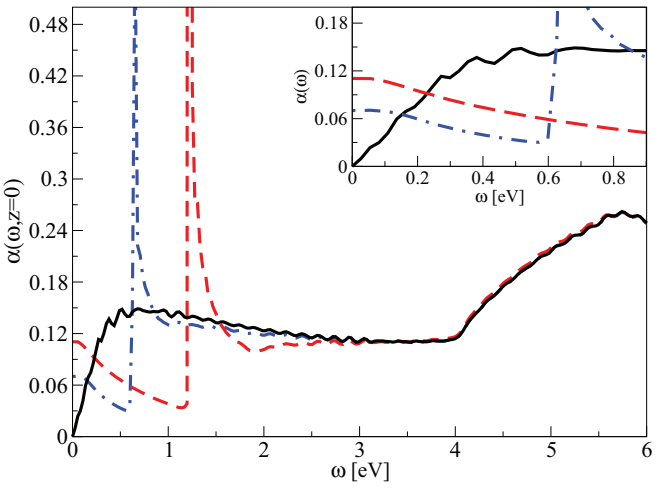

FIG. 8. (Color online) Singularity indices in pristine (black solid line), doped $E_F = 0.5$ eV (blue dash-dotted line), and doped $E_F = 1$ eV (red dashed line) graphene. The inset shows the behavior of singularity indices in the low-energy ($\omega \approx 0$) limit.

241 k points, and it agrees with previous calculations.[19] For the graphene unit cell parameter we used the experimental value $a = 4.651$ a.u. and for the unit cell in z direction (separation between periodically repeated graphene layers) we take $L = 5a = 23.255$ a.u. as is shown in Fig. 1. For the response function it will be important to choose the right thickness of the electron density, which we have taken to be $2a$, as shown in Fig. 1.

B. Response function calculation

The independent electron response function matrix for quasi-two-dimensional systems can be written as

$$\chi^0_{\mathbf{G}_\parallel\mathbf{G}'_\parallel}(\mathbf{Q},\omega,z,z') = \frac{2}{S}\sum_{\mathbf{K}\in S.B.Z.}\sum_{n,m}\frac{f_n(\mathbf{K}) - f_m(\mathbf{K}+\mathbf{Q})}{\omega + i\eta + E_n(\mathbf{K}) - E_m(\mathbf{K}+\mathbf{Q})} \times M_{n\mathbf{K},m\mathbf{K}+\mathbf{Q}}(\mathbf{G}_\parallel,z)\, M^*_{n\mathbf{K},m\mathbf{K}+\mathbf{Q}}(\mathbf{G}'_\parallel,z'), \quad (23)$$

where S is the normalization surface, and in the summation over $\mathbf{K}$ we have used $101 \times 101 \times 1$ K-point mesh sampling, which corresponds to 10 303 Monkhorst-Pack special k points in the Brillouin zone and 901 in the irreducible Brillouin zone. Also, n,m summation is carried out over 20 bands, which proved to be enough for the proper description of the high-energy $\pi + \sigma$ plasmon. The damping parameter η used in this calculation is 100 meV. The matrix elements in Eq. (23) have the form

$$M_{n\mathbf{K},m\mathbf{K}+\mathbf{Q}}(\mathbf{G}_\parallel,z) = \langle\Phi_{n\mathbf{K}}|e^{-i(\mathbf{Q}+\mathbf{G}_\parallel)\boldsymbol{\rho}}|\Phi_{n\mathbf{K}+\mathbf{Q}}\rangle_S, \quad (24)$$

where $\mathbf{Q}$ and $\mathbf{G}_\parallel$ are the momentum transfer vector and reciprocal lattice vector, respectively, parallel to the x-y plane, and the integration is performed over the normalization surface S. The plane wave expansion of the wave function has the form

$$\Phi_{n\mathbf{K}}(\boldsymbol{\rho},z) = \frac{1}{\sqrt{V}}e^{i\mathbf{K}\boldsymbol{\rho}}\sum_{\mathbf{G}} C_{n\mathbf{K}}(\mathbf{G})e^{i\mathbf{G}\mathbf{r}},$$

where $V = S * L$ is the normalization volume, $\mathbf{G} = (\mathbf{G}_\parallel, G_z)$ are three-dimensional (3D) reciprocal vectors, $\mathbf{r} = (\boldsymbol{\rho}, z)$ is the 3D position vector and the coefficients $C_{n\mathbf{K}}$ are obtained by solving the KS equations. It should be noted that the integration over perpendicular z coordinate in the expression (24) is still not performed, so the matrix elements are z dependent. The RPA response function can be obtained from the independent electron response function (23) by solving the Dyson equation

$$\chi_{\mathbf{G}_\parallel\mathbf{G}'_\parallel}(\mathbf{Q},\omega,z,z') = \chi^0_{\mathbf{G}_\parallel\mathbf{G}'_\parallel}(\mathbf{Q},\omega,z,z') + \sum_{\mathbf{G}_{\parallel 1}}\int_{-L/2}^{L/2} dz_1 dz_2\, \chi^0_{\mathbf{G}_\parallel\mathbf{G}_{\parallel 1}}(\mathbf{Q},\omega,z,z_1) \times V(\mathbf{Q}+\mathbf{G}_{\parallel 1},z_1,z_2)\, \chi_{\mathbf{G}_{\parallel 1}\mathbf{G}'_\parallel}(\mathbf{Q},\omega,z_2,z'), \quad (25)$$

where $V(\mathbf{Q},z,z') = \frac{2\pi}{Q}e^{-Q|z-z'|}$ is a 2D Fourier transform of a 3D bare Coulomb interaction. Here it is important to note that the z_1,z_2 integrations in Eq. (25) are performed within only one of the periodically repeated unit cells in the z direction, so the Coulomb interaction with other unit cells is excluded.

After Fourier expansion of $\chi(z,z')$

$$\chi_{\mathbf{G}_\parallel\mathbf{G}'_\parallel}(\mathbf{Q},\omega,z,z') = \frac{1}{L}\sum_{G_zG'_z}\chi_{\mathbf{G}\mathbf{G}'}(\mathbf{Q},\omega)e^{iG_zz - iG'_zz'} \quad (26)$$

and similarly for $\chi^0(z,z')$, Eq. (25) becomes a full matrix equation

$$\chi_{\mathbf{G}\mathbf{G}'}(\mathbf{Q},\omega) = \chi^0_{\mathbf{G}\mathbf{G}'}(\mathbf{Q},\omega) + \sum_{\mathbf{G}_1\mathbf{G}_2}\chi^0_{\mathbf{G}\mathbf{G}_1}(\mathbf{Q},\omega)V_{\mathbf{G}_1\mathbf{G}_2}(\mathbf{Q})\chi_{\mathbf{G}_1\mathbf{G}'}(\mathbf{Q},\omega), \quad (27)$$

where the Coulomb interaction matrix elements have the explicit form

$$V_{\mathbf{G}_1\mathbf{G}_2}(\mathbf{Q}) = \frac{4\pi}{|\mathbf{Q}+\mathbf{G}_1|^2}\delta_{\mathbf{G}_1\mathbf{G}_2} - p_{G_{z1}}p_{G_{z2}}\frac{4\pi(1-e^{-|\mathbf{Q}+\mathbf{G}_{\parallel 1}|L})}{|\mathbf{Q}+\mathbf{G}_{\parallel 1}|L} \times \frac{|\mathbf{Q}+\mathbf{G}_{\parallel 1}|^2 - G_{z1}G_{z2}}{\left(|\mathbf{Q}+\mathbf{G}_{\parallel 1}|^2+G^2_{z1}\right)\left(|\mathbf{Q}+\mathbf{G}_{\parallel 1}|^2+G^2_{z2}\right)}\delta_{\mathbf{G}_{\parallel 1}\mathbf{G}_{\parallel 2}}, \quad (28)$$

where

$$p_{G_z} = \begin{cases} 1; & G_z = \frac{2k\pi}{L} \\ -1; & G_z = \frac{(2k+1)\pi}{L} \end{cases}, \quad k = 0,1,2,3,\ldots.$$

The solution of Eq. (27) has the form

$$\chi_{\mathbf{G}\mathbf{G}'}(\mathbf{Q},\omega) = \sum_{\mathbf{G}_1}\mathcal{E}^{-1}_{\mathbf{G}\mathbf{G}_1}(\mathbf{Q},\omega)\chi^0_{\mathbf{G}_1\mathbf{G}'}(\mathbf{Q},\omega), \quad (29)$$

where we have introduced the dielectric matrix

$$\mathcal{E}_{\mathbf{G}\mathbf{G}'}(\mathbf{Q},\omega) = \delta_{\mathbf{G}\mathbf{G}'} - \sum_{\mathbf{G}_1}V_{\mathbf{G}\mathbf{G}_1}(\mathbf{Q})\chi^0_{\mathbf{G}_1\mathbf{G}'}(\mathbf{Q},\omega). \quad (30)$$

The screened Coulomb interaction then can be written as

$$W_{\mathbf{G}_\parallel}(\mathbf{Q},\omega,z,z') = \delta_{\mathbf{G}_\parallel 0}v(\mathbf{Q},z,z') + W^{\mathrm{ind}}_{\mathbf{G}_\parallel}(\mathbf{Q},\omega,z,z'), \quad (31)$$

where the induced or dynamical part of the Coulomb interaction can be written in terms of matrix elements of the response matrix (29)

$$W^{\mathrm{ind}}_{\mathbf{G}_\parallel}(\mathbf{Q},\omega,z,z') = \int_{-L/2}^{L/2} dz_1 dz_2 v(\mathbf{Q}+\mathbf{G}_\parallel,z,z_1) \times \chi_{\mathbf{G}_\parallel 0}(\mathbf{Q},\omega,z_1,z_2)\, v(\mathbf{Q},z_2,z'). \quad (32)$$

After the Fourier transformation in real space the propagator of the induced Coulomb interaction becomes

$$W^{\mathrm{ind}}(\mathbf{r},\mathbf{r}',\omega) = \sum_{\mathbf{G}_\parallel}\int\frac{d\mathbf{Q}}{(2\pi)^2}\, e^{i(\mathbf{G}_\parallel+\mathbf{Q})\boldsymbol{\rho}}\, e^{-i\mathbf{Q}\boldsymbol{\rho}'} \times W^{\mathrm{ind}}_{\mathbf{G}_\parallel}(\mathbf{Q},\omega,z,z'). \quad (33)$$

For the RPA response function calculation we have taken the unit cell thickness $L = 23.255$ a.u., which corresponds to five unit cell parameters in the parallel direction. We have neglected crystal local field effects in the parallel but not in the perpendicular direction. We have used the energy of 20 Hartrees as the cutoff for Fourier expansion over G_z's which corresponds to 47 G_z vectors. This cutoff proved to be sufficient to give a smooth, monotonically decaying tail of the induced charge density for $z > a$.

V. DYNAMICAL SINGULARITY INDEX IN PRISTINE AND DOPED GRAPHENE

In this section we compare the dynamical singularity index $\alpha(\mathbf{R},\omega)$ calculated using a properly screened potential with the approximations and predictions presented in Sec. III. In the calculation of the spectrum we shall take only the $\mathbf{G}_{\parallel} = 0$ term in Eq. (15), so that the parallel coordinate $\boldsymbol{\rho}$ becomes unimportant, and $z = 0$. Once we have calculated the function $\alpha(\omega)$ we shall also be able to calculate the complete spectrum given by Eq. (16).

As expected, numerically calculated functions $\alpha(\omega)$ confirm our predictions of their qualitative behavior in the asymptotic ($\omega \to 0$) limit, though they differ appreciably for higher frequencies where the details of the band structure become important. In Fig. 8 we see that in the asymptotic limit for pristine graphene $\alpha(\omega)$ goes to zero, while for the doped graphene ($E_F = 0.5$ and 1 eV) it has a finite value. In fact, the validity of the asymptotic expression $\alpha_0(\omega)$ is strongly restricted. For $E_F = 0$ the singularity index $\alpha(\omega)$ indeed starts from zero, but very soon, on the scale of the core-hole linewidth γ, it increases due to $\pi \to \pi^*$ interband transitions. The asymptotic quadratic behavior is immediately modified due to the energy-dependent screened interaction, assumed to be constant in the expression (18). On the other hand, for $E_F = 0.5$ and 1 eV the $\alpha(\omega)$ starts at finite value, as predicted by the asymptotic result (18), which would indicate singular behavior, but it immediately decreases as the $\pi \to \pi$ intraband transitions decrease, and a new collective mode gives a strong peak at the 2D plasmon frequency.[22] At even higher energies interband $\pi \to \pi^*$ transitions dominate, and give the same contributions for all graphene dopings. We can compare these results with those for a 3D metal,[20] where $\alpha(\omega)$ is quite constant in a larger ω region almost up to the appearance of the first plasmon peak. Strong variation of $\alpha(\omega)$ in graphene could lead to the core-hole lineshapes showing a combined effect of singular-hole relaxation and hole decay processes, which all occur in the same energy region, as we shall see in Sec. VII.

VI. CALCULATION OF THE CORE-HOLE SPECTRA

Once we have calculated the function $\alpha(\mathbf{R},\omega)$ we can calculate the complete spectrum given by Eq. (16), e.g., the core-hole energy shift ΔE and the strength of the no-loss line P_0. Let us first analyze the case $\beta = 0$, i.e., for $\alpha(\omega) \sim$ const. for $\omega \to 0$. It turns out that expanding the exponent in Eq. (16) is not a satisfactory procedure because already the first term in the expansion

$$A(\omega) = P_0\delta(\tilde{\omega}) + P_0\frac{\alpha(\tilde{\omega})}{\tilde{\omega}} + \cdots, \tag{34}$$

where $\tilde{\omega} = \omega - \tilde{E}$, would vanish, and the expansion (34) is therefore meaningless. If we approximate $\alpha(\omega)$ by its asymptotic (constant) value $\alpha = \alpha(0)$, we can calculate the spectrum (16) analytically to obtain the Doniach-Šunjić (DS) asymmetric lineshape[3]

$$A_{DS}(\tilde{\omega}) = \frac{1}{\pi}\frac{\Gamma(1-\alpha)\cos\left[\frac{\pi\alpha}{2} + (1-\alpha)\arctan\left(\frac{\tilde{\omega}}{\gamma}\right)\right]}{(\tilde{\omega}^2+\gamma^2)^{(1-\alpha)/2}} \tag{35}$$

with the maximum at

$$\tilde{\omega}_{\max} = \gamma\ \cot\frac{\pi}{2-\alpha}.$$

Incidentally, this maximum is not the shifted elastic line (which is suppressed in this case), but corresponds to the inelastic structure due to a large number of soft electron-hole pairs. This expression is correct only in the low-energy (e.g., $\omega < E_F$) part of the spectrum. However, this is not possible for the frequency-dependent $\alpha(\omega)$, so we shall instead use a more general approach.[8,13] We first notice that the core-hole Green's function (12) satisfies the equation

$$\left\{i\frac{\partial}{\partial t} - \tilde{E} + i\gamma\right\} G(t) = \delta(t) + G(t)\int_0^\infty d\nu\ \alpha(\nu)e^{-i\nu t}. \tag{36}$$

After Fourier transformation we obtain an integral equation for the Green's function

$$G(\tilde{\omega}) = G_0(\tilde{\omega}) + G_0(\tilde{\omega})\int_0^\infty d\nu\ \alpha(\nu)G(\tilde{\omega}-\nu), \tag{37}$$

which can be separated into real and imaginary parts G_R and G_I, respectively,

$$G_R(\tilde{\omega}) = G_{0R}(\tilde{\omega})\left[1 + J_R(\tilde{\omega})\right] - G_{0I}(\tilde{\omega})\,J_I(\tilde{\omega}), \tag{38}$$

$$G_I(\tilde{\omega}) = G_{0I}(\tilde{\omega})\left[1 + J_R(\tilde{\omega})\right] + G_{0R}(\tilde{\omega})\,J_I(\tilde{\omega}), \tag{39}$$

where

$$J_{R,I}(\tilde{\omega}) = \int_0^\infty d\nu\alpha(\nu)\,G_{R,I}(\tilde{\omega}-\nu)$$

and

$$G_{0R}(\tilde{\omega}) = \frac{\tilde{\omega}}{\tilde{\omega}^2+\gamma^2},\quad G_{0I}(\tilde{\omega}) = -\frac{\gamma}{\tilde{\omega}^2+\gamma^2}. \tag{40}$$

Equations (38) and (39) can be solved by using the iterative procedure which starts with G_0 given by Eq. (40). The core-hole spectra can be calculated from

$$A(\tilde{\omega}) = -\frac{1}{\pi}G_I(\tilde{\omega}) \tag{41}$$

with G_I obtained self-consistently from Eqs. (38) and (39), and for the singularity index $\alpha(\nu)$ calculated from Eq. (15). This method enables us to calculate the whole normalized spectrum, but we shall first analyze the strength of the no-loss peak, i.e., the $\tilde{\omega} = 0$ pole contribution to the spectrum in the Lorentzian form

$$A_0(\tilde{\omega}) = \frac{1}{\pi}\frac{\gamma}{\tilde{\omega}^2+\gamma^2}.$$

From Eq. (39) one finds

$$A(\tilde{\omega}\to 0) \to Z(\gamma)\,A_0(\tilde{\omega})$$

for the decay constant γ, where $Z(\gamma)$ is the strength of the residuum,

$$Z(\gamma) = 1 + J_R(\tilde{\omega} = 0),$$

or alternatively,

$$Z(\gamma) = \pi\gamma\,A(\tilde{\omega} = 0).$$

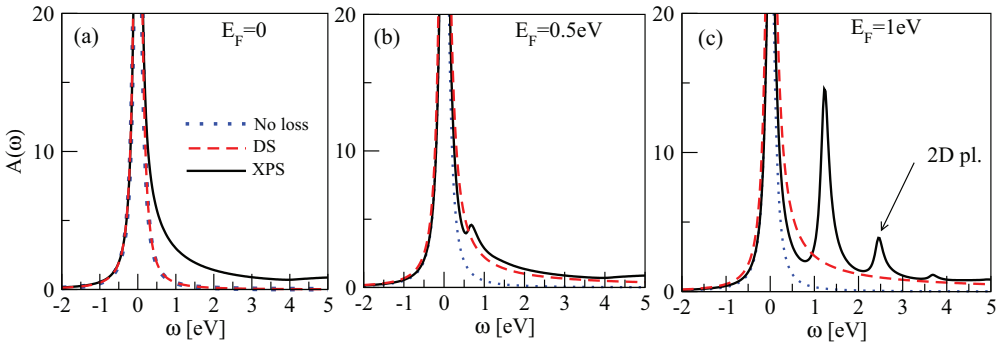

FIG. 9. (Color online) (a) XPS core-hole spectra in pristine graphene (black solid line); DS lineshape (red dashed line); no-loss line (blue dotted line). (b) The same as for (a) for doped graphene ($E_F = 0.5$ eV). (c) The same as for (a) for doped graphene ($E_F = 1$ eV). Hole decay constant γ is taken to be 100 meV.

VII. DISCUSSION

In Fig. 9 we show the core-hole spectra calculated using the formalism of Sec. VI for pristine graphene ($E_F = 0$) and for two dopings, $E_F = 0.5$ and 1 eV. In pristine graphene $\alpha(0) = 0$, so the DS lineshape $A_{DS}(\omega)$ reduces to the Lorentzian $A_0(\omega)$. However, if we depart from this approximation and calculate the spectrum with the full $\alpha(\omega)$, we obtain a noticeable low-energy tail, which is due to the interband $\pi \to \pi^*$ transitions, as is visible in a rapid increase of $\alpha(\omega)$ in Fig. 8. It is easy to mistake it for a singular many-electron tail, i.e., to interpret the lineshape in Fig. 9(a) as the DS lineshape, e.g., in Fig. 9(b). To clarify this, in Fig. 10 we reproduce the full XPS spectrum from Fig. 9(a), but also the contribution from first-order processes only. We see that they give the dominant contribution to this low-energy tail.

For finite doping, in Figs. 9(b) and 9(c) the DS lineshape given by Eq. (35) shows a pronounced asymmetry due to $\pi^* \to \pi^*$ intraband transitions, increasing with doping. However, the full calculation modifies this asymptotic result as the series of discrete 2D plasmon peaks appears in Fig. 9(c) at energies 1.2, 2.4, and 3.6 eV.

Important information about the strength of many-electron excitations can be obtained from the strength of the no-loss line $Z(\gamma, E_F)$, which depends on the doping E_F and the hole decay constant γ, and is shown in Fig. 11. We see that the elastic line is fully destroyed only for extremely small hole decay constants γ, but even for realistic values it is substantially reduced, indicating strong inelastic scattering which amounts to 40–50% of the total spectral weight.

Another related quantity confirming this conclusion is the ground-state energy shift ΔE, Eq. (14), which is connected to the total inelastic spectrum by the spectral sum rule (17), so that

$$\Delta E = \int d\omega \omega A_{\text{inel}}(\omega), \tag{42}$$

where $A_{\text{inel}}(\omega) = A(\omega) - A_0(\omega)$. Figure 12 shows the core-hole energy shift as a function of the core-hole position and graphene doping. First we observe that the core-hole energy shift does not depend on the hole decay constant γ, as can be shown analytically from Eq. (16). When the core-hole is outside graphene (beyond the graphene electronic density edge) the energy shift follows the image potential curves (taken from Ref. 21) up to very close distances (4 a.u. from the graphene center) and is mostly due to the long-range $\pi \to \pi^*$ derived plasmon excitations. At shorter distances, as one would expect, the quantum mechanical dispersion reduces the polarization shift. The energy shift in the center of the graphene (black dots) is smaller than at the image plane

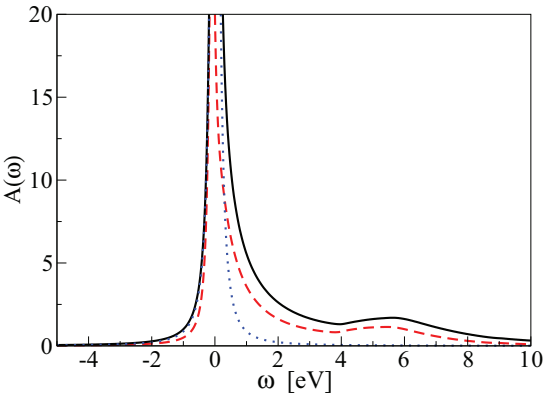

FIG. 10. (Color online) Comparison between the no-loss line A_0 (blue dotted line), first-order spectral function A_1 (red dashed line), and full spectral function A (black solid line).

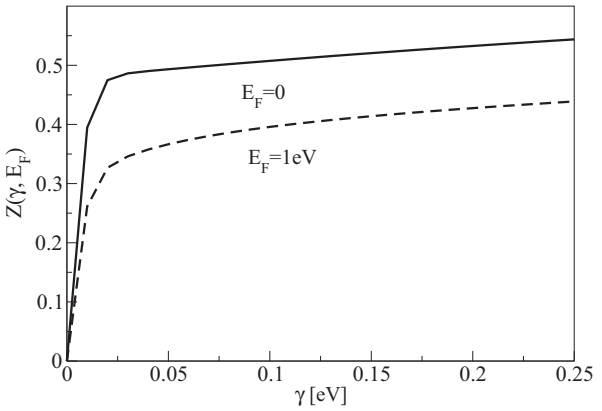

FIG. 11. The strength of the no-loss line as function of hole decay constant γ for pristine graphene $E_F = 0$ (solid line) and doped graphene $E_F = 1$ eV (dashed line).

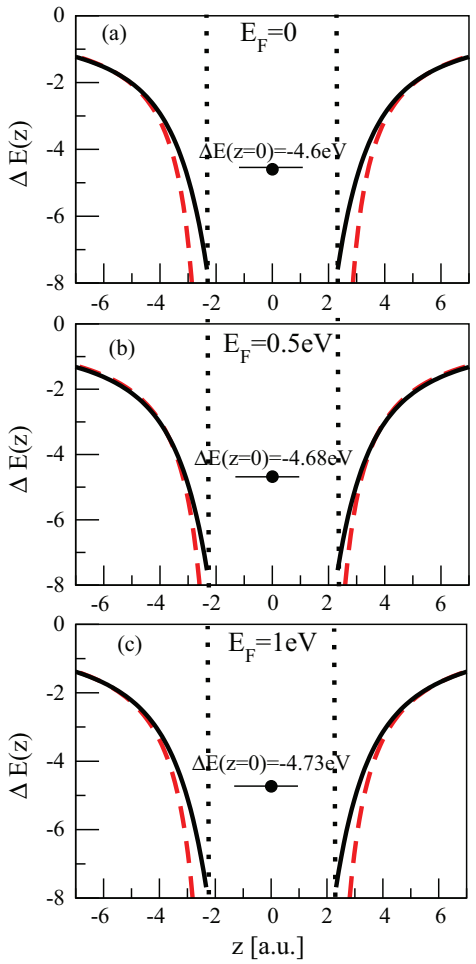

FIG. 12. (Color online) Core-hole energy shift as a function of its z position (black solid line) in (a) pristine graphene, (b) doped graphene $E_F = 0.5$ eV, and (c) doped graphene $E_F = 1$ eV. Corresponding image potential fit (red dashed line) is taken from Ref. 21 Dotted vertical lines denote the graphene image plane positions, and the black dot represents the core-hole energy shift in the center of graphene.

position (vertical dotted lines). This behavior is expected, namely the maximum energy shift should appear exactly at the centroid of the induced charge which is for graphene at $z_{im} \approx 2$ a.u. (Ref. 21). This induced charge originates mainly from the transitions between π and π^* orbitals. On the other hand, π orbitals have nodes exactly at the graphene center and that is the reason why the energy shift at the graphene center behaves as for the core hole just outside graphene. We notice that the energy shifts in the center of graphene, like the effective image plane position z_{im}, very weakly depend on graphene doping.

Let us now compare these theoretical predictions with the experimental observation of singular lineshapes in graphene. Photoemission spectra involving C1s line in graphene have been reported in a number of papers,[23–28] but the primary purpose of these measurements was to determine structural, chemical, or transport properties, growth mechanisms, the influence of substrate or temperature on these properties, and so on. Nevertheless, in several cases measured lineshapes were fitted to the DS asymmetric profiles,[23,24,27,28] and even singularity indices were determined.[23,24]

So Gruneis *et al.*[23] fitted the measured C1s spectrum to the DS lineshape with $\gamma = 216$ meV and $\alpha_0 = 0.1$, which is compatible with the earlier results found in Ref. 24 for graphene monolayers deposited on various metallic substrates, where DS lineshapes were also used with α_0 between 0.1 and 0.18. No doping was assumed nor discussed in these papers, though it should play an important role in determining the asymmetry and possible singular character of core-hole lineshapes. Also one should consider the influence of the substrate on deposited graphene monolayer.

The influence of the substrate can be twofold. On one hand, it could lead to the charge transfer and doping of the graphene monolayer. On the other, if the substrate is metallic, the hole in the graphene monolayer can interact with the electrons in the substrate, and also show singular lineshapes, as was shown by the authors of Ref. 13. All these factors should be taken into account when trying to determine whether the observed asymmetry is due to the singular excitation of electron-hole pairs, or to low-order scattering processes. In any case, it turns out that the observed asymmetry of the C1s line cannot be directly related to the doping in graphene, and more systematic experiments will be needed to resolve this interesting issue.

ACKNOWLEDGMENTS

The authors are grateful to Donostia International Physics Center (DIPC) and Pedro M. Echenique for the hospitality during various stages of this research.

*vito@phy.hr

[1] G. D. Mahan, Phys. Rev. **163**, 612 (1967).
[2] P. Nozieres and C. T. De Dominicis, Phys. Rev. **178**, 1097 (1969).
[3] S. Doniach and M. Sunjić, J. Phys. C **3**, 285 (1970).
[4] P. W. Anderson, Phys. Rev. Lett. **18**, 1049 (1967).
[5] D. C. Langreth, Phys. Rev. B **1**, 471 (1970).
[6] M. Combescot and P. Nozieres, J. Phys. (Paris) **32**, 913 (1971).
[7] G. D. Mahan, Phys. Rev. B **11**, 4814 (1975).
[8] P. Minnhagen, Phys. Lett. A **56**, 327 (1976); J. Phys. F **7**, 2441 (1977).
[9] P. Minnhagen, J. Phys. F **6**, 1789 (1976).
[10] K. D. Schotte and U. Schotte, Phys. Rev. **182**, 479 (1969).
[11] P. H. Citrin, Phys. Rev. B **8**, 5545 (1973).
[12] P. H. Citrin, G. K. Wertheim, and M. Schluter, Phys. Rev. B **20**, 3067 (1979).
[13] V. Despoja, M. Šunjić, and L. Marušić, Phys. Rev B **77**, 035424 (2008).
[14] G. D. Mahan, *Many-Particle Physics*, 2nd ed. (Pergamon, New York, 1990).

[15]P. Giannozzi, S. Baroni, N. Bonini, M. Calandra, R. Car, C. Cavazzoni, D. Ceresoli, G. L. Chiarotti, M. Cococcioni, I. Dabo, A. D. Corso, Stefano de Gironcoli, S. Fabris, G. Fratesi, R. Gebauer, U. Gerstmann, C. Gougoussis, A. Kokalj, M. Lazzeri, L. Martin-Samos, N. Marzari, F. Mauri, R. Mazzarello, S. Paolini, A. Pasquarello, L. Paulatto, C. Sbraccia, S. Scandolo, G. Sclauzero, A. P. Seitsonen, A. Smogunov, P. Umari, and R. M. Wentzcovitch, J. Phys.: Conden. Matter **21**, 395502 (2009).

[16]J. P. Perdew and A. Zunger, Phys. Rev. B **23**, 5048 (1981).

[17]N. Troullier and J. L. Martins, Phys. Rev. B **43**, 1993 (1991).

[18]V. Despoja, D. Novko, K. Dekanić, M. Šunjić, and L. Marušić, Phys. Rev. B **87**, 075447 (2013).

[19]P. E. Trevisanutto, C. Giorgetti, L. Reining, M. Ladisa, and V. Olevano, Phys. Rev. Lett. **101**, 226405 (2008); C. Attaccalite, A. Grüeneis, T. Pichler, and A. Rubio, arXiv:0808.0786v2.

[20]E. Muller-Hartman, T. V. Ramakrishnan, and G. Toulouse, Phys. Rev. B **3**, 1102 (1971).

[21]V. Despoja, D. J. Mowbray, D. Vlahović, and L. Marušić, Phys. Rev. B **86**, 195429 (2012).

[22]E. H. Hwang and S. Das Sarma, Phys. Rev. B **75**, 205418 (2007).

[23]A. Gruneis, K. Kummer, and D. V. Vyalikh, New J. Phys. **11**, 073050 (2009).

[24]A. B. Preobrajenski, May Ling Ng, A. S. Vinogradov, and N. Martensson, Phys. Rev. B **78**, 073401 (2008).

[25]M. J. Webb, P. Palmgren, P. Pal, O. Karis, and H. Grennberg, Carbon **49**, 3242 (2011).

[26]Wei Zhao, Sergey M. Kozlov, O. Hofert, K. Gotterbarm, Michael P. A. Lorenz, F. VinÌes, C. Papp, A. Gorling, and Hans-Peter Steinruck, J. Phys. Chem. Lett. **2**, 759 (2011).

[27]A. Pirkle, J. Chan, A. Venugopal, D. Hinojos, C. W. Magnuson, S. McDonnell, L. Colombo, E. M. Vogel, R. S. Ruoff, and R. M. Wallace, Appl. Phys. Lett. **99**, 122108 (2011).

[28]C. Mattevi, G. Eda, S. Agnoli, S. Miller, K. Andre Mkhoyan, O. Celik, D. Mastrogiovanni, G. Granozzi, E. Garfunkel, and M. Chhowalla, Adv. Funct. Mater. **19**, 2577 (2009).